Elastic Instability behind Brittle Fracture

D. Riccobelli, P. Ciarletta, G. Vitale, C. Maurini, L. Truskinovsky

Elastic instability behind brittle fracture

D. Riccobelli,[1] P. Ciarletta,[1] G. Vitale,[2] C. Maurini,[3] and L. Truskinovsky[4,*]

[1] *MOX – Dipartimento di Matematica, Politecnico di Milano, 20133 Milano, Italy*
[2] *Laboratoire de Mecanique des Solides, École Polytechnique, 91128 Palaiseau, France.*
[3] *CNRS, Institut Jean Le Rond d'Alembert, Sorbonne Université, UMR 7190, 75005 Paris, France.*
[4] *ESPCI ParisTech, PMMH, CNRS – UMR 7636, 75005 Paris, France.*

We argue that nucleation of brittle cracks in initially flawless soft elastic solids is preceded by a nonlinear elastic instability, which cannot be captured without accounting for geometrical precise description of finite elastic deformation. As a prototypical problem we consider a homogeneous elastic body subjected to tension and assume that it is weakened by the presence of a free surface which then serves as a site of crack nucleation. We show that in this maximally simplified setting, brittle fracture emerges from a symmetry breaking elastic instability activated by softening and involving large elastic rotations. The implied bifurcation of the homogeneous elastic equilibrium is highly unconventional for nonlinear elasticity as it exhibits an extraordinary sensitivity to geometry, reminiscent of the transition to turbulence in fluids. We trace the post-bifurcational development of this instability beyond the limits of applicability of scale free continuum elasticity and use a phase-field approach to capture the scale dependent sub-continuum strain localization, signaling the formation of actual cracks.

While linearized elasticity theory is usually sufficient in problems involving *propagation* of pre-existing cracks [1–3], we present a compelling evidence that, at least for some classes of soft materials, the description of crack *nucleation* requires an account of both geometrically and physical elastic nonlinearity [4, 5]. To elucidate the physical origin of the failure of linear theory, we build a continuous path from surface instability in tension to fracture.

The phenomenon of *surface fracture* is of considerable recent interest because the sub-micron parts employed in many modern applications are effectively defect free and their fracture usually originates on unconstrained external surfaces [6]. Crack nucleation at the surface is also of importance for the understanding of the fragmentation of various brittle surface layers [7–10]. More generally, the emergence of surface fracture patterns [11, 12] is an example of a symmetry breaking instability which is at the heart of complexity development from soft matter physics [13, 14] to biophysics [15, 16].

Nonlinear elastic instabilities were studied extensively in the context of *compressive* buckling [17–25]. Elastic instabilities can also take place under tension, with necking, wrinkling and shear banding, as the most prominent examples [26–30]. However, the potential relation of these *tensile* instabilities to fracture has been largely overlooked. Several studies attempted to develop conceptual links between the bulk crack nucleation and material softening and used them to advance various phenomenological nucleation criteria [11, 31–38]. Still, an understanding of how such criteria relate to the subtle interplay between geometric and physical nonlinearities along the crack nucleation path remains obscure.

Brittle cracking of soft solids is not uncommon, as it is exemplified by an abrupt failure of an elastic rubber band under tension. In particular, *brittle-soft* behavior is characteristic for hydrogels [39–42], where the diverging stress at the crack tip is typically accompanied not only by large stretches but also by large rotations with several candidate mechanisms debated as potential regulators of the underlying material failure at the micro scale [43].

In this Letter we use the geometrically simplest setting to explore both linear and nonlinear stages of the tensile instability in a soft solid which culminates in the formation of a brittle crack. The implied instability is of *spinodal* type [39–41] but with a peculiarity that it is associated with the surface rather than with the bulk [42–46]. The degenerate nature of this instability in the purely elastic setting [47] leads to a high sensitivity of the emerging patterns to sample geometry. Such sensitivity is typical for nonlinear systems without an internal length scale and therefore the ensuing crack nucleation scenario is reminiscent, for instance, of a transition to turbulence. Regularization of the problem, bringing a fixed internal length scale, naturally simplifies the picture, as it is already known from the study of the prototypical one dimensional models [48, 49].

Our first goal is to show in detail how the above symmetry breaking elastic instability serves as a precursor of the ultimate strain localization. Then, since the emerging strain singularity renders the scale-free continuum elasticity inadequate, the modeling paradigm must be changed if the goal is to capture the formation of sharp cracks. To describe the role of micro-scales in such a sharpening process we resort to a phase-field-type extension of the continuum theory [34, 48, 50, 51]. We show that such a hybrid approach allows one to model seamlessly the whole process from a continuum elastic instability to a sub-continuum evolution of developed cracks.

Consider a 2D rectangular body $\Omega = [-L,\, L] \times [0,\, H]$. Denote by $\mathbf{x} \in \Omega$ points in the reference configuration and by $\mathbf{y}(\mathbf{x})$ their deformed position, see Fig. 1. Working directly with the deformation gradient $\mathsf{F} = \nabla \mathbf{y}$ we ac-

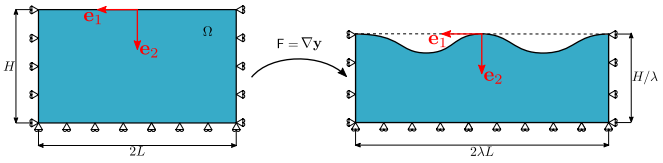

FIG. 1. Schematic representation of the considered surface instability showing the reference and the actual configurations, while also detailing the nature of the boundary conditions.

count for *geometric* nonlinearities. In such an approach not only the principal stretches $\lambda_{1,2}$ (the square roots of the eigenvalues of $\mathsf{F}^T\mathsf{F}$), can be large but also that the description of rotations is geometrically exact [18].

Assume that the material is incompressible, so that $\det \mathsf{F} = \lambda_1\lambda_2 = 1$, and isotropic, so that the elastic energy density can be written as $\hat{w}(\lambda_1) = w(\lambda_1, \lambda_1^{-1})$. We can then write the force balance in the form $\nabla \cdot \mathsf{P} = 0$, where P_{ij} are the components of the first Piola-Kirchhoff stress tensor $\mathsf{P} = \partial w/\partial \mathsf{F} + p\mathsf{F}^{-1}$ and p is the Lagrange multiplier enforcing the incompressibility constraint.

Suppose further that the body Ω is loaded in a two-sided hard device, such that $y_1 = \lambda x_1$ at $x_1 = \pm L$, where λ is the applied stretch which serves as the control parameter. Then on the side boundaries (at $x_1 = \pm L$) the horizontal displacements are prescribed $y_1 = \pm\lambda L$ while the possibility of free sliding is ensured by the second condition $P_{12} = 0$. The upper boundary $x_2 = 0$ will be kept free so that $P_{22} = P_{21} = 0$ while the lower boundary $x_2 = H$ will be constrained only partially so that $y_2 = H/\lambda$ and $P_{21} = 0$. The ensuing basic problem of elasticity theory admits a homogeneous solution $\mathbf{y^{(0)}} := \mathsf{F^{(0)}}\mathbf{x}$, where $\mathsf{F}^{(0)} = \mathrm{diag}\,(\lambda, \lambda^{-1})$; the corresponding pressure is $p^{(0)} := -\lambda^{-1}\partial w/\partial\lambda_2$.

To study the stability of this solution, we use standard methods [20, 52–54] and write the perturbed displacement and pressure fields, in the form $\mathbf{y} = \mathbf{y}^{(0)} + \sum_{j=1}^{\infty} \varepsilon^j \mathbf{u}^{(j)}$ and $p = p^{(0)} + \sum_{j=1}^{\infty} \varepsilon^j p^{(j)}$ where ε is a small parameter. Inserting these expansions in the force balance we obtain, at the first order, a linear boundary value problem for $\mathbf{u}^{(1)}$ and $p^{(1)}$.

To illustrate the results we introduce the stream function $\mathbf{u}^{(1)}(\mathbf{x}) = (\partial_{\mathbf{2}}\chi, -\partial_{\mathbf{1}}\chi)$, and write the solution of the first order equilibrium problem in the form $\chi = iAg(\gamma x_2)\exp(i\gamma x_1)/\gamma + \text{c.c.}$, where A is still undefined complex amplitude and c.c. denotes complex conjugate. Here we have also introduced the horizontal wavenumber $\gamma = (n\pi)/(2\lambda L)$, where n is an integer with even (odd) values representing symmetric (asymmetric) modes, respectively. The expression for $p^{(1)}(\mathbf{x})$ in terms of $g(\gamma x_2)$ is too long to be presented here, see [55].

Following closely [20], we write the real valued function g in the form $g(\gamma x_2) = \sum_{k=1}^{4} C_k \exp[\gamma\omega_k\, x_2]$, where $\omega_1 = -\omega_2 = \alpha$, $\omega_3 = -\omega_4 = \beta$. The constants α, β can be found from the relations $\alpha\beta = \lambda^2$ and $\alpha^2 + \beta^2 + 2 = \lambda(\lambda^4 - 1)\eta$; the elastic energy enters these relations through the function $\eta(\lambda) = \hat{w}''(\lambda)/\hat{w}'(\lambda)$ which characterizes the *physical* nonlinearity.

The bifurcation points $\lambda_n(H/L)$, parametrized by the integers $n(H/L)$, can be found from the condition that there exists a nontrivial set of coefficients C_k, such that the functions $\mathbf{u}^{(1)}$ and $p^{(1)}$) satisfy the boundary conditions at the linear order. This gives an explicit nonlinear algebraic equation, see [55]. We can then define $\lambda_{\mathrm{cr}}(H/L) = \min_{n\geq 1} \lambda_n(H/L)$ and denote by $n_{\mathrm{cr}}(H/L)$ the corresponding critical mode. To illustrate the sensitivity of the instability threshold $\lambda_{\mathrm{cr}}(H/L)$ to the geometry of the domain characterized by the ratio H/L, we need to choose a specific energy density.

To account for strain softening in the simplest form, we assume that $w = \mu\,(I-2)/I$, where $I = \lambda_1^2 + \lambda_2^2$ is the first strain invariant and μ is the measure of rigidity (see more about this particular choice in [55]). In this case $\hat{w}(\lambda) = \mu(\lambda^2-1)^2/(2(\lambda^4+1))$ and the softening ($\hat{w}'' < 0$) takes place for $\lambda > \lambda_{\mathrm{lm}} = \sqrt[4]{(1/3)\left(\sqrt{33}+6\right)}$, see Fig. 2(a) and [55]. The value λ_{lm} is known as the Considère or the load maximum (LM) threshold [54, 62, 63], where by the 'load' we understand the axial stress in the direction of traction $P(\lambda) = \mathbf{e}_1 \cdot \mathsf{P} \cdot \mathbf{e}_1 = \hat{w}'(\lambda)$; reaching this threshold indicates the occurrence of necking in slender bodies [20, 26, 64, 65]; it can be shown that crossing the LM threshold is also a necessary condition for the occurrence of a general instability [20].

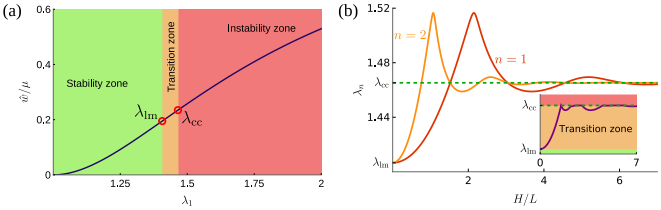

FIG. 2. (a) The energy density $\hat{w}(\lambda)$ of our softening material as a function of the maximal principal stretch λ_1. (b) The stability curves for the two modes with $n = 1, 2$; the purple line in the inset represents the function $\lambda_{\mathrm{cr}}(H/L)$.

Observe first that, independently of the value of n, the functions $\lambda_n(H/L)$, shown in Fig. 2(b) for $n = 1, 2$, approach the point $\lambda_{\mathrm{lm}} \simeq 1.407$ in the limit infinitely small aspect ratios ($H \ll L$, thin domains) and the point $\lambda_{\mathrm{cc}} \simeq 1.465$ in the limit of infinitely large aspect ratios ($H \gg L$, thick domains).

Note that the emerging threshold λ_{cc} indicates the failure of the complementing condition (CC) [44, 46, 66–68]. In an infinite system it marks the onset of wrinkling instability with all wave numbers becoming unstable simultaneously. In our case the value of the CC threshold can be found analytically as a solution of the transcendental equation $\eta(\lambda_{\mathrm{cc}}) = -\lambda_{\mathrm{cc}}^{-3}$ [55]. Note also that in the classical geometrically linearized elasticity theory, where both

stretches and rotations are small and therefore we can use the approximation $w(\mathsf{E})$ with $\mathsf{E} = (1/2)(\nabla\mathbf{u} + \nabla\mathbf{u}^T)$, the very difference between the thresholds $\lambda_{\rm cc}$ and $\lambda_{\rm lm}$ disappears and the whole complexity of the emerging stability diagram is lost [55].

Outside these two limits (of infinitely thin and infinitely thick domains), the behavior of the function $\lambda_{\rm cr}(H/L)$ looks uncorrelated. However, a remarkable underlying structure reveals itself if we focus instead on the integer valued function $n_{\rm cr}(H/L)$, see Fig.3.

First of all, we observe that the necking-type instability with $n_{\rm cr} = 1$ is not a feature of slender bodies only, but appears periodically as one changes the aspect ratio. Similarly, the wrinkling-type instability with $n_{\rm cr} = \infty$ appears at periodically distributed values of the aspect ratio. In both cases the period is the same and is equal to $\Delta(H/L) = 4\lambda_{\rm cc}^3/\sqrt{-1 + 2\lambda_{\rm cc}^2 + 3\lambda_{\rm cc}^4}$, see [55] for details.

Overall, we observe a periodic distribution of 'staircase' structures with infinite number of steps in every period representing all integer values of $n_{\rm cr}$ from necking with $n_{\rm cr} = 1$ to wrinkling with $n_{\rm cr} = \infty$. Each of these 'staircases' demonstrates the same 'devilish' features with step accumulation taking place around the recurrent wrinkling thresholds (where the unstable mode becomes singularly localized near the free surface). In other words, each 'staircase ' describes a scale-free crossover between necking and wrinkling with the steps emerging due to the locking in the parameter intervals where horizontal and vertical oscillations of the displacement field are resonant with the domain geometry. To the best of our knowledge, the reported extreme sensitivity of the critical wave number to the aspect ratio and the emergence of special geometries where the instability pattern changes dramatically from fully localized to fully de-localized, have not been previously observed in nonlinear elasticity problems.

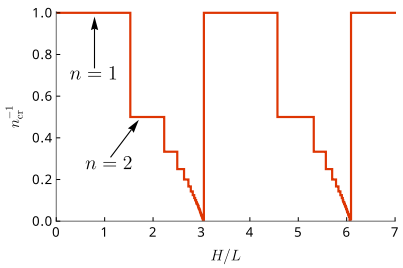

FIG. 3. The inverse of the critical mode $n_{\rm cr}$ versus the aspect ratio H/L.The accumulation points correspond to $n = \infty$.

The revealed distribution of the stability thresholds can be corroborated analytically using the observation that for $H/L \gg 1$ (when $\lambda_{\rm cr} \sim \lambda_{\rm cc}$) one can approximate the actual problem of finding $n_{\rm cr}(H/L)$, involving minimization of an implicitly given function over a discrete set, by a model problem $N = \arg\max_\xi(\sin(a\xi)/e^\xi)$, where ξ is a positive integer and $a \sim H/L$. The model problem can be solved explicitly and its solution N can be formally proved to exhibit the periodic staircase structure of the type shown in Fig. 3.

To determine the nature of detected bifurcations, we now perform a standard weakly nonlinear amplitude expansion [4, 69–75]. The idea is to compute the next terms of the perturbative expansion $\mathbf{u}^{(2)}$, $p^{(2)}$ and use the obtained information to determine λ dependence of the amplitude A near the bifurcation point $\lambda_{\rm cr}$. In this respect the 'near necking' (single-mode instability) and the 'near wrinkling' (multi-mode instability) regimes function differently.

Indeed, in the more conventional 'near necking' regimes, where the buckling thresholds λ_n are well separated and only a finite number of modes are initially activated in the postbuckling regime, the natural small parameter is known to be $\varepsilon = \sqrt{|\lambda - \lambda_{\rm cr}|/\lambda_{\rm cr}}$. By expanding the energy functional $\mathcal{W} = \int_\Omega w\,{\rm d}\mathbf{x}$ in ε we obtain [55] $\Delta\mathcal{W} = \varepsilon^4(\theta_2 |A|^2 + \theta_4 |A|^4) + o(\varepsilon^4)$, where $\theta_2(\lambda)$, $\theta_4(\lambda)$ are known real functions. The requirement of stationarity of the energy in A (at order ε^4), gives the expression for the amplitude $A = \sqrt{-\theta_2/(2\theta_4)}$ where θ_2 and θ_4 have the same sign. This characterizes the bifurcation as a subcritical (unstable) pitchfork, see the dashed line in Fig. 4 (a). The implied unstable postbuckling regime is the diffuse necking illustrated in the inset in Fig. 4(a).

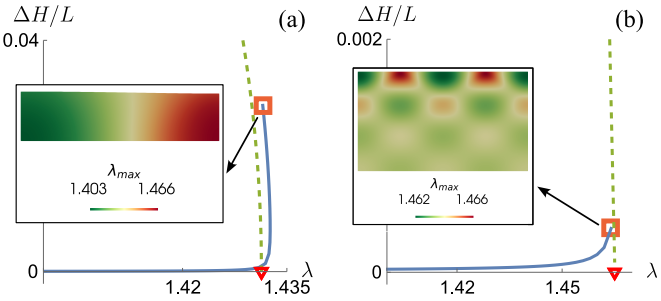

FIG. 4. Bifurcation diagrams showing the amplitude ΔH of the unstable mode on the free surface for the cases: (a) $H/L = 1$ (near necking case) and (b) $H/L = 2.5$ (near wrinkling case). The red triangles denote the critical thresholds $\lambda_{\rm cr}$. Solid and dashed lines represent the results of the finite element simulations and of the weakly non-linear analysis, respectively. Insets show the distribution of the maximal principal stretch $\lambda_{\rm max}$ in the actual configuration corresponding to the location of the square marker.

The 'near wrinkling' regimes, where buckling thresholds accumulate, are markedly different. In this case a small increment of the control parameter λ away from the critical value $\lambda_{\rm cr}$ activates an essentially infinite number of instability modes. Therefore in the weakly nonlinear approximation an unstable mode interacts with many other modes. The availability of a broad bandwidth of such modes requires a different scaling and one can show that the natural small parameter in this case

is $\varepsilon = |\lambda - \lambda_{\rm cr}|/\lambda_{\rm cr}$, see [76, 77] for similar analyses. To take into account all the implied interactions we need to modify the expression for the first order stream function adopted in the 'near necking' case and write instead $\chi = \sum_{m=-\infty}^{+\infty} i(A_m/\gamma m) g(\gamma m x_2) \exp(i\gamma m x_1) + \text{c.c.}$ where m is an integer and A_m is amplitude of the mode m. We can then proceed as before and find the amplitude equation, accounting for cubic resonances, which now takes the form of an infinite system: $\theta_1 A_m + \sum_{k=-\infty}^{+\infty} \theta_{3(k)} A_k A_{m-k} = 0$. Here the real functions $\theta_1(\lambda; m)$ and $\theta_{3(k)}(\lambda; m)$ are known explicitly [55]. The analysis shows that the bifurcation is again a subcritical pitchfork, see the dashed line in Fig. 4(b), which implies that the incipient postbifurcational mode, illustrated in the inset in Fig. 4(b) is again unstable.

To complement this analytical study we also performed some parallel direct numerical simulations. For numerical convenience we slightly modified the model by introducing into our original energy density $w(\mathsf{F})$ a dependence on $J = \lambda_1\lambda_2$, a measure of volumetric deformation. More specifically we used the expression $w_J(\mathsf{F}) = (\mu/I)\,(I - 2\log J - 2) + (\Lambda/2)(\log J)^2$ with Λ equal to 100μ which corresponds to almost incompressibility; note that at $\Lambda \to +\infty$ we recover both the original model.

The bifurcated branch was recovered after we introduced a small imperfection on the free boundary with a wavenumber of the instability mode and a small amplitude of the order of $10^{-5}\,L$, see the blue lines in Fig. 4(a,b). We used an arclength continuation method [78, 79] which allowed us to reach the state of strain focusing caused the local violation of the complementing condition. The deformation patterns at such limits (of the applicability of continuum elasticity) are illustrated in the insets in Fig. 4(a,b) for the typical 'near necking' and 'near wrinkling' regimes.

The ultimate strain localization, which caused the break down of our continuum model, is indicative of the trend towards the formation of atomically sharp cracks. To capture the latter, the scale-free continuum theory, which is expected to be operative only on long waves, can be regularized through the introduction of a sub-continuum length scale. A convenient approach of this type is a phase-field model of fracture, e.g. [50, 51, 80, 81]. Specifically, we assume that

$$w_{\rm pf}(\mathsf{F}, \alpha) = (1-\alpha)^2(\mu/2)(I-2) + \mu\alpha^2 + \mu\,\ell_0^2\|\nabla\alpha\|^2,$$

where $\alpha(\mathbf{x}) \in [0,1]$ is a subcontinuum damage-like scalar field: the compatibility with our original nonlinear elasticity model is ensured by the fact that $w(\mathsf{F}) = \min_{\alpha\in[0,1]}[(1-\alpha)^2(\mu/2)(I-2) + \mu\alpha^2]$. The regularization is achieved through the term penalizing gradients of α which brings an internal length scale ℓ_0. At $\ell_0 \ll L$ this approach is known to be equivalent to the Griffith fracture model with the toughness $G_c = \mu\ell_0/2$ [34, 50, 82].

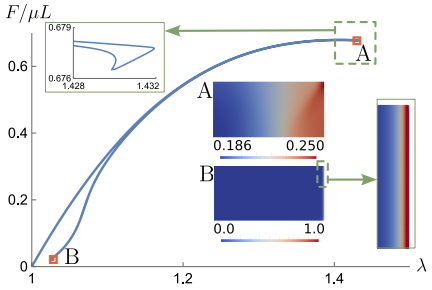

FIG. 5. Normalized axial force $F/\mu L$ versus the mean stretch λ for the near necking case ($H/L = 1$). The insets on the right show the distribution of the internal variable α in the reference configuration corresponding to the points A and B. The parameter $\ell_0/H = 0.01$.

Going in this way beyond continuum elasticity and adopting again the weak compressibility regularization, we performed a series of numerical simulations with the goal to capture the actual formation of cracks. We used a Newton's algorithm complemented by a standard pseudo-arclength continuation technique [78] to minimize at each value of the loading parameter λ the energy with respect to both, the deformation field $\mathbf{y}(\mathbf{x})$ and the auxiliary scalar field $\alpha(\mathbf{x})$.

The results of the two representative numerical simulations, illustrating qualitatively different 'near necking' and 'near wrinkling' regimes, are presented in Figs. 5-6. In both figures the (unstable) post-bifurcational response is represented through the dimensionless force-stretch relation $F(\lambda) = \int_{-H}^{0} P_{11}(\lambda)|_{x_1=L}\,dx_2$. The deformed configurations close and far from the bifurcation points are shown in the insets. Note that while in our 'near wrinkling' regime we show for simplicity only the case with two emerging cracks, the aspect ratio of the domain and the regularization length could be chosen differently to obtain arbitrary many cracks.

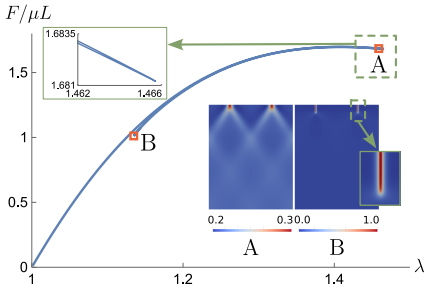

FIG. 6. Normalized axial force $F/\mu L$ versus the mean stretch λ for the near wrinkling case ($H/L = 2.5$). The insets on the right show the distribution of the internal variable α in the reference configuration corresponding to the points A and B. The parameter $\ell_0/H = 0.01$.

The common feature of the two cases, shown in Figs. 5-6, is the gradual sharpening of the initially diffuse local

'non-affinity' measured by parameter α. The actual formation of cracks can be linked to the moment of reaching the value $\alpha \sim 1$ inside the localized regions with the thickness of order of sub-continuum scale ℓ_0. Since the focus of our study is crack nucleation, we did not advance our simulations till the complete break down of the slab which is preceded by secondary bifurcations representing both crack branching and crack arrest [11]. Overall, the presence in this problem of a subcritical bifurcation indicates the possibility of abrupt (dynamic) transition from a homogeneous state to a cracked state which is a typical scenario in brittle fracture.

To conclude, using the simplest geometrical setting and focusing on initially flawless soft solids, we showed that crack nucleation is preceded by an elastic instability which can be identified using continuum elasticity theory only if the latter accounts properly for both geometrical and physical nonlinearities. Such elasticity theory predicts a surprisingly complex linear stability diagram with recurrent geometry-sensitive crossovers between necking and wrinkling modes. Both necking and wrinkling instabilities were shown to evolve towards the formation of developed cracks when the classical elasticity was seamlessly extended as a phase-field type model. Our analysis builds a bridge between nonlinear elasticity and fracture mechanics and points to the existence of purely elastic precursors of crack nucleation. Similar mechanisms should be operative in other highly nonlinear manifestations of elasticity such as cavitation [83, 84], phase nucleation [85, 86], and creasing [87, 88].

DR and PC gratefully acknowledge partial support from grant Dipartimento di Eccellenza 2023-2027 and MIUR, PRIN 2017 Project "Mathematics of active materials: From mechanobiology to smart devices". DR has been partially supported by MIUR, PRIN 2022 Project "Mathematical models for viscoelastic biological matter". DR and PC are members of the INdAM research group GNFM. This work was performed using HPC resources from GENCI-IDRIS (Grant 2023-AD010913451R1).

* lev.truskinovsky@espci.fr

[1] L. D. Landau, E. M. Lifshitz, A. M. Kosevich, and L. P. Pitaevskii, *Theory of elasticity: volume 7*, Vol. 7 (Elsevier, 1986).
[2] D. Broek, *The practical use of fracture mechanics* (Springer Science & Business Media, 2012).
[3] K. B. Broberg, *Cracks and fracture* (Elsevier, 1999).
[4] S. S. Antman, *Nonlinear Problems of Elasticity* (Springer, 2005) pp. 513–584.
[5] J. M. Marsden and T. J. R. Hughes, *Mathematical Foundations of Elasticity* (Prentice-Hall Inc., 1983).
[6] G. Dehm, B. N. Jaya, R. Raghavan, and C. Kirchlechner, Acta Mater. **142**, 248 (2018).
[7] J. W. Hutchinson and Z. Suo, Adv. Appl. Mech. **29**, 63 (1991).
[8] H. Colina, L. de Arcangelis, and S. Roux, Phys. Rev. B **48**, 3666 (1993).
[9] U. Handge, Y. Leterrier, G. Rochat, I. Sokolov, and A. Blumen, Phys. Rev. E **62**, 7807 (2000).
[10] H. Alarcón, O. Ramos, L. Vanel, F. Vittoz, F. Melo, and J.-C. Géminard, Physical review letters **105**, 208001 (2010).
[11] B. Bourdin, J.-J. Marigo, C. Maurini, and P. Sicsic, Phys. Rev. Lett. **112**, 014301 (2014).
[12] L. Truskinovsky, G. Vitale, and T. Smit, Int. J. Eng. Sci. **83**, 124 (2014).
[13] J. Kim, J. Yoon, and R. C. Hayward, Nat. Mater. **9**, 159 (2010).
[14] E. Hohlfeld and L. Mahadevan, Phys. Rev. Lett. **106**, 10.1103/PhysRevLett.106.105702 (2011).
[15] M. B. Amar and A. Goriely, J. Mech. Phys. Solids **53**, 2284 (2005).
[16] P. Ciarletta, V. Balbi, and E. Kuhl, Phys. Rev. Lett. **113**, 248101 (2014).
[17] M. A. Biot, *Mechanics of Incremental Deformations* (John Wiley & Sons, 1965).
[18] R. W. Ogden, *Non-Linear Elastic Deformations* (Dover, 1984).
[19] D. Bigoni, *Nonlinear Solid Mechanics: Bifurcation Theory and Material Instability* (Cambridge University Press, 2012).
[20] R. Hill and J. Hutchinson, J. Mech. Phys. Solids **23**, 239 (1975).
[21] G. DelPiero and R. Rizzoni, J. Elast. **93**, 203 (2008).
[22] J. Sivalogathan and S. Spector, Proc. R. Soc. **466**, 1167 (2012).
[23] Y. Grabovsky and L. Truskinovsky, Contin. Mech. Thermodyn. **19**, 211 (2007).
[24] K. Sawyers and R. Rivlin, J. Elast. **12**, 101 (1982).
[25] N. Triantafyllidis, W. M. Scherzinger, and H.-J. Huang, Int. J. Solids Struct. **44**, 3700 (2007).
[26] B. Audoly and J. W. Hutchinson, J. Mech. Phys. Solids **97**, 68 (2016).
[27] Q. Li and T. J. Healey, J. Mech. Phys. Solids **97**, 260 (2016).
[28] E. Cerda and L. Mahadevan, Phys. Rev. Lett. **90**, 074302 (2003).
[29] J. W. Hutchinson and V. Tvergaard, Int. J. Solids Struct. **17**, 451 (1981).
[30] R. Hill and J. Hutchinson, J. Mech. Phys. Solids **23**, 239 (1975).
[31] P. Klein and H. Gao, Eng. Fract. Mech. **61**, 21 (1998).
[32] S. A. Silling, O. Weckner, E. Askari, and F. Bobaru, Int. J. Fract. **162**, 219 (2010).
[33] A. Shekhawat, S. Zapperi, and J. P. Sethna, Phys. Rev. Lett. **110**, 185505 (2013).
[34] E. Tanné, T. Li, B. Bourdin, J.-J. Marigo, and C. Maurini, J. Mech. Phys. Solids **110**, 80 (2018).
[35] A. Kumar, B. Bourdin, G. A. Francfort, and O. Lopez-Pamies, J. Mech. Phys. Solids **142**, 104027 (2020).
[36] P. K. Kristensen, C. F. Niordson, and E. Martínez-Pañeda, Phil. Trans. R. Soc. A **379**, 20210021 (2021).
[37] T. Hao and Z. M. Hossain, Phys. Rev. B **100**, 014204 (2019).
[38] C. J. Larsen, Mech. Res. Commun. **128**, 104059 (2023).
[39] C. J. Gagne, H. Gould, W. Klein, T. Lookman, and A. Saxena, Phys. Rev. Lett. **95**, 095701 (2005).
[40] A. O. Schweiger, K. Barros, and W. Klein, Phys. Rev. E

75, 031102 (2007).
[41] W. Klein, T. Lookman, A. Saxena, and D. M. Hatch, Phys. Rev. Lett. **88**, 085701 (2002).
[42] H. C. Simpson and S. J. Spector, J. Elast. **15**, 229 (1985).
[43] A. Benallal, R. Billardon, and G. Geymonat, in *Bifurcation and Stability of Dissipative Systems* (Springer, 1993) pp. 1–44.
[44] H. C. Simpson, J. Elast. **139**, 1 (2020).
[45] A. Mielke and P. Sprenger, J. Elast. **51**, 23 (1998).
[46] P. V. Negrón-Marrero and E. Montes-Pizarro, J. Elast. **107**, 151 (2012).
[47] S. G. Mikhlin, Russ. Math. Surv. **28**, 45 (1973).
[48] O. U. Salman and L. Truskinovsky, J. Mech. Phys. Solids **154**, 104517 (2021).
[49] A. Gupta and T. J. Healey, J. Elast. , 1 (2023).
[50] B. Bourdin, G. Francfort, and J.-J. Marigo, J. Mech. Phys Solids **48**, 797 (2000).
[51] A. Karma, D. A. Kessler, and H. Levine, Phys. Rev. Lett. **87**, 045501 (2001).
[52] Y. Cao and J. W. Hutchinson, Proc. R. Soc. A **468**, 94 (2012).
[53] M. A. Holland, B. Li, X. Q. Feng, and E. Kuhl, J. Mech. Phys. Solids **98**, 350 (2017).
[54] J. Li, H. Varner, and T. Cohen, J. Mech. Phys. Solids **172**, 105171 (2023).
[55] See Supplemental Material [url] for the details of the computations, which includes Refs. [56–61].
[56] F. Charru, *Hydrodynamic instabilities*, Vol. 37 (Cambridge University Press, 2011).
[57] Y. B. Fu and P. Ciarletta, Proc. R. Soc. A **471**, 20140979 (2015).
[58] M. Alnæs, J. Blechta, J. Hake, A. Johansson, B. Kehlet, A. Logg, C. Richardson, J. Ring, M. E. Rognes, and G. N. Wells, Archive of Numerical Software **3**, 9 (2015).
[59] D. Riccobelli, G. Noselli, and A. DeSimone, Proc. R. Soc. A **477**, 20200817 (2021).
[60] S. Balay, S. Abhyankar, M. Adams, P. Brune, K. Buschelman, L. Dalcin, W. Gropp, B. Smith, D. Karpeyev, D. Kaushik, *et al.*, *Petsc users manual revision 3.7*, Tech. Rep. (Argonne National Lab.(ANL), Argonne, IL (United States), 2016).
[61] P. Chadwick and R. W. Ogden, Arch. Rational Mech. Anal. **44**, 54 (1971).
[62] I. S. Yasnikov, A. Vinogradov, and Y. Estrin, Scr. Mater. **76**, 37 (2014).
[63] S. M. Fielding, Phys. Rev. Lett. **107**, 258301 (2011).
[64] V. Tvergaard, Comput. Methods Appl. Mech. Eng. **103**, 273 (1993).
[65] A. Needleman, Mech. Mater. **116**, 180 (2018).
[66] M. Šilhavý, *The Mechanics and Thermodynamics of Continuous Media* (Springer Berlin Heidelberg, 1997).
[67] X. Liu and B.-W. Schulze, *Boundary Value Problems with Global Projection Conditions*, Vol. 265 (Springer, 2018).
[68] M. A. Biot, Appl. Sci. Res. **12**, 168 (1963).
[69] P. Becherer, A. N. Morozov, and W. van Saarloos, Physica D **238**, 1827 (2009).
[70] M. Weinstein, Proc. R. Soc. A **375**, 155 (1981).
[71] B. Audoly, Phys. Rev. E **84**, 011605 (2011).
[72] Y. Pomeau, S. Zaleski, and P. Manneville, Phys. Rev. A **27**, 2710 (1983).
[73] W. T. Koiter, *On the stability of elastic equilibrium* (National Aeronautics and Space Administration, 1967).
[74] B. Budiansky, Adv. Appl. Mech. **14**, 1 (1974).
[75] A. M. A. van der Heijden, ed., *W. T. Koiter's Elastic Stability of Solids and Structures* (Cambridge University Press, 2008).
[76] Y. B. Fu and R. W. Ogden, Contin. Mech. Thermodyn. **11**, 141 (1999).
[77] P. Ciarletta and Y. Fu, Int. J. Non-Linear Mech. **75**, 38 (2015).
[78] R. Seydel, *Practical bifurcation and stability analysis*, Vol. 5 (Springer Science & Business Media, 2009).
[79] Y. Su, D. Riccobelli, Y. Chen, W. Chen, and P. Ciarletta, Proc. R. Soc. A **479**, 20230358 (2023).
[80] I. S. Aranson, V. A. Kalatsky, and V. M. Vinokur, Phys. Rev. Lett. **85**, 118 (2000).
[81] L. Eastgate, J. Sethna, M. Rauscher, T. Cretegny, C.-S. Chen, and C. Myers, Physical review E **65**, 036117 (2002).
[82] A. A. Griffith, Phil. Trans. R. Soc. Lond. **221**, 163 (1921).
[83] J. M. Ball, Phil. Trans. R. Soc. Lond. A **306**, 557 (1982).
[84] A. Kumar and O. Lopez-Pamies, J. Mech. Phys. Solids **150**, 104359 (2021).
[85] T. J. Healey and U. Miller, Proc. R. Soc. A **463**, 1117 (2007).
[86] Y. Grabovsky and L. Truskinovsky, J. Nonlinear Sci. **23**, 891 (2013).
[87] P. Ciarletta and L. Truskinovsky, Phys. Rev. Lett. **122**, 248001 (2019).
[88] S. S. Pandurangi, A. Akerson, R. S. Elliott, T. J. Healey, and N. Triantafyllidis, J. Mech. Phys. Solids **160**, 104749 (2022).

Elastic instability behind brittle fracture: Supplemental Material

D. Riccobelli,[1] P. Ciarletta,[1] G. Vitale,[2] C. Maurini,[3] and L. Truskinovsky[4,*]

[1] *MOX – Dipartimento di Matematica, Politecnico di Milano, 20133 Milano, Italy*
[2] *Laboratoire de Mecanique des Solides, École Polytechnique, 91128 Palaiseau, France.*
[3] *CNRS, Institut Jean Le Rond d'Alembert, Sorbonne Université, UMR 7190, 75005 Paris, France.*
[4] *ESPCI ParisTech, PMMH, CNRS – UMR 7636, 75005 Paris, France.*

Linear stability analysis

At the linear order the incremental Piola–Kirchhoff stress is of the form $\mathsf{P}^{(1)} = \mathbf{K}^{(1)} : \mathsf{\Gamma} - p^{(0)}\mathsf{\Gamma} + p^{(1)}\mathsf{I}$ where $\mathsf{\Gamma} = \nabla_{\mathbf{x}}\mathbf{u}^{(1)}$, $\nabla_{\mathbf{x}}$ is the gradient operator in the finitely deformed configuration $[-\lambda L,\, \lambda L] \times [0,\, H/\lambda]$, and $\mathbf{K}^{(1)}$ is the tensor of instantaneous elastic moduli. The components of $\mathbf{K}^{(1)}$ are given by [1]

$$
\begin{aligned}
K^{(1)}_{iijj} &= \lambda_i\lambda_j \frac{\partial^2 W}{\partial\lambda_i\partial\lambda_j},\\
K^{(1)}_{ijij} &= \frac{\left(\lambda_i \dfrac{\partial W}{\partial\lambda_i} - \lambda_j \dfrac{\partial W}{\partial\lambda_j}\right)\lambda_i^2}{\lambda_i^2 - \lambda_j^2}, \quad i \neq j,\\
K^{(1)}_{ijji} &= K^{(1)}_{jiij} = K^{(1)}_{ijij} - \lambda_i \frac{\partial W}{\partial\lambda_i}, \quad i \neq j,
\end{aligned}
$$

for $i, j = 1, 2$. At the linear order, the incremental equations can be written as $\nabla_{\mathbf{x}} \cdot \mathsf{P}^{(1)} = 0$, $\operatorname{tr}\mathsf{\Gamma} = 0$, which are complemented by the linearized form of the boundary conditions: $\mathbf{u}^{(1)} \cdot \mathbf{e}_2 = 0$ at$x_2 = H/\lambda$; $\mathbf{e}_1 \cdot {\mathsf{P}^{(1)}}^T \mathbf{e}_2 = 0$ at $x_2 = H/\lambda$; $\mathbf{u}^{(1)} \cdot \mathbf{e}_1 = 0$ at $x_1 = \pm\lambda L$; $\mathbf{e}_2 \cdot {\mathsf{P}^{(1)}}^T \mathbf{e}_1 = 0$ at $x_1 = \pm\lambda L$ and finally $\mathsf{P}^{(1)}\mathbf{e}_2 = \mathbf{0}$ at $x_2 = 0$. As explained in the main text, it is natural to look for solutions in the form

$$
u_1^{(1)} = \imath A g'(\gamma x_2) e^{\imath\gamma x_1} + c.c., \qquad u_2^{(1)} = A g(\gamma x_2) e^{\imath\gamma x_1} + c.c., \tag{S1}
$$

$$
p^{(1)} = \gamma A((K^{(1)}_{1122} + K^{(1)}_{2112} - K^{(1)}_{1111}) g'(\gamma x_2) + K^{(1)}_{2121} g'''(\gamma x_2)) e^{\imath\gamma x_1} + c.c., \tag{S2}
$$

with the scalar function g given in this general form

$$
g(\gamma x_2) = C_1 \cosh(\alpha\gamma x_2) + C_2 \sinh(\alpha\gamma x_2) + C_3 \cosh(\beta\gamma x_2) + C_4 \sinh(\beta\gamma x_2). \tag{S3}
$$

Here C_1, C_2, C_3, C_4 are constants to be found from the boundary conditions, while α and β satisfy

$$
\alpha^2 = \frac{b}{c} + \sqrt{\left(\frac{b}{c}\right)^2 - \frac{a}{c}}, \;\; \beta^2 = \frac{b}{c} - \sqrt{\left(\frac{b}{c}\right)^2 - \frac{a}{c}}, \tag{S4}
$$

where

$$
\begin{aligned}
a = K^{(1)}_{1212} &= \lambda^5 \frac{w'(\lambda)}{\lambda^4 - 1}, \quad c = K^{(1)}_{2121} = \lambda \frac{w'(\lambda)}{\lambda^4 - 1},\\
2b = K^{(1)}_{1111} + K^{(1)}_{2222} - 2(K^{(1)}_{1122} + K^{(1)}_{2112}) &= \lambda^2 w''(\lambda) - 2c.
\end{aligned} \tag{S5}
$$

The non trivial solutions of the resulting linear system exists whenever the following characteristic equation for the eigenvalue γ is satisfied

$$
\begin{aligned}
&\left(\alpha^4\beta + 2\alpha^3\beta^2 + 2\alpha^2\left(\beta^3 + \beta\right) + \alpha\left(\beta^4 + 2\beta^2 - 1\right) - \beta\right)(\alpha - \beta)^2 \sinh\left(\frac{H\gamma(\alpha + \beta)}{\lambda}\right) +\\
&+(\alpha + \beta)^2\left(\alpha^4\beta - 2\alpha^3\beta^2 + 2\alpha^2\left(\beta^3 + \beta\right) - \alpha\left(\beta^4 + 2\beta^2 - 1\right) - \beta\right)\sinh\left(\frac{H\gamma(\alpha - \beta)}{\lambda}\right) = 0.
\end{aligned} \tag{S6}
$$

The corresponding eigenfunction g can be then written in the form:

$$g(\gamma x_2) = \cosh(\alpha\gamma x_2) - \frac{\cosh(\alpha\gamma h) - \frac{\alpha^2+1}{\beta^2+1}\cosh(\beta\gamma H/\lambda)}{\sinh(\alpha\gamma H/\lambda) - \frac{\beta^2+1}{\alpha^2+1}\frac{\alpha}{\beta}\sinh(\beta\gamma H/\lambda)}\cosh(\beta\gamma x_2) + \\ -\frac{\alpha^2+1}{\beta^2+1}\sinh(\alpha\gamma x_2) + \frac{\frac{\beta^2+1}{\alpha^2+1}\cosh(\alpha\gamma H/\lambda) - \cosh(\beta\gamma H/\lambda)}{\frac{\alpha}{\beta}\sinh(\alpha\gamma H/\lambda) - \frac{\beta^2+1}{\alpha^2+1}\sinh(\beta\gamma H/\lambda)}\sinh(\beta\gamma x_2). \tag{S7}$$

Material behavior

To achieve analytical transparency, we consider the strain energy density of a softening solid in the following simple form

$$w(\mathsf{F}) = \frac{\mu}{I}(I-2) = \mu\frac{\left(\lambda_1^2-1\right)^2}{\lambda_1^4+1}, \tag{S8}$$

where $I = \mathsf{F} : \mathsf{F} = \lambda_1^2 + \lambda_1^{-2}$. For the homogeneous deformation $\mathsf{F}^{(0)} = \mathrm{diag}(\lambda, \lambda^{-1})$, the strain energy density reduces to the function $w(\lambda)$. The load maximum (LM) stretch $\lambda_{\rm lm}$ introduced in the main text and corresponding to the maximum of $w'(\lambda)$ is now $\lambda_{\rm lm} = \sqrt[4]{\frac{1}{3}\left(\sqrt{33}+6\right)}$. The complementing condition (CC) is violated whenever the incremental problem admits a non-trivial solution in the half-space. Therefore, by taking the limit $H \to +\infty$, in the characteristic equation (S6) we obtain an equation for $\lambda = \lambda_{\rm cc}$:

$$\lambda_{\rm cc}^3 w''(\lambda_{\rm cc}) + w'(\lambda_{\rm cc}) = 0. \tag{S9}$$

In the case of the strain energy density (S8), the equation (S9) reads $3\lambda_{\rm cc}^{11} - \lambda_{\rm cc}^9 - 12\lambda_{\rm cc}^7 + \lambda_{\rm cc}^3 + \lambda_{\rm cc} = 0$, and its relevant root is $\lambda_{\rm cc} \simeq 1.46527$.

The formal advantage of the choice (S8) for $W(\mathsf{F})$ becomes clear at the very end of our study where we take advantage of the fact that such an energy density can be obtained as the minimum of a function involving the auxiliary field α characterizing material softening:

$$w(\mathsf{F}) = \min_{\alpha\in[0,1]} \psi(\alpha, \mathsf{F}) = \min_{\alpha\in[0,1]} a(\alpha)\widehat{w}(\mathsf{F}) + \phi(\alpha), \tag{S10}$$

where $\widehat{w}(\mathsf{F}) = \frac{\mu}{2}(I-2) = \frac{\mu}{2}\left(\lambda_1^2 + \lambda_1^{-2} - 2\right)$ is the strain energy density of a standard neo-Hookean material, $a(\alpha) = (1-\alpha)^2$ is the measure of stiffness degradation and $\phi(\alpha) = \mu\alpha^2$ is the energetic price of such degradation.

Periodicity of stability thresholds

Assume that the thresholds $\lambda_{\rm cc} > \lambda_{\rm lm} > 1$ exist for a given strain energy density $w(\lambda_1)$ and suppose that $\lambda \in [\lambda_{\rm lm}, \lambda_{\rm cc}]$. Then from (S9) we have $\eta(\lambda) \in \left[-1/\lambda^3, 0\right]$. Then $(\alpha+\beta)^2 > 0$, $(\alpha-\beta)^2 < 0$, while $\alpha\beta$ is real and positive. Therefore, α and β are complex conjugate numbers and we can write $\alpha = \gamma + \imath\delta, \qquad \beta = \gamma - \imath\delta, \qquad \gamma, \delta > 0$, with $\delta = \delta(\lambda)$, $\gamma = \gamma(\lambda)$, whose explicit expressions can be easily obtained. The characteristic equation (S6) can be now rewritten as

$$\sin(\tilde{A}n) = f(\lambda, n). \tag{S11}$$

where

$$\tilde{A}(\lambda) = \frac{\pi\delta(\lambda)}{\lambda^2}\frac{H}{L}, \qquad f(\lambda, n) = \frac{\delta\left(1+\lambda^3\eta(\lambda)\right)}{\gamma\left(1-\lambda^3\eta(\lambda)\right)}\sinh\left(\frac{\pi\gamma n}{\lambda^2}\frac{H}{L}\right). \tag{S12}$$

We observe that $f(\lambda_{\rm cc}, n) = 0$ for any value of n. The corresponding values of the aspect ratio are

$$\frac{H}{L} = \frac{m\lambda^2}{\delta(\lambda_{\rm cc})} = \frac{2m\lambda_{\rm cc}^3}{\sqrt{3\lambda_{\rm cc}^4 + 2\lambda_{\rm cc}^2 - 1}}.$$

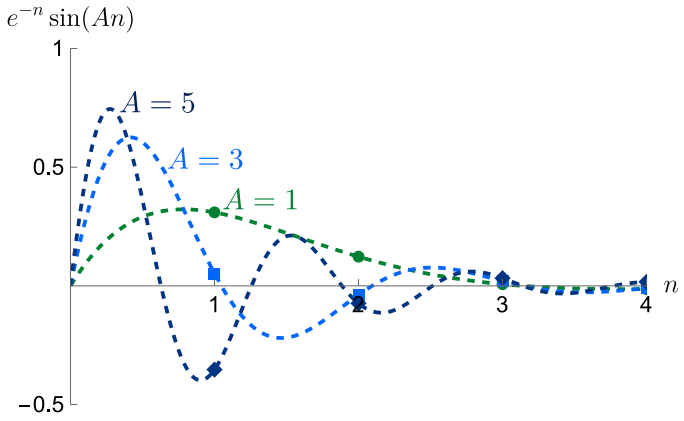

FIG. S1. The function $e^{-n}\sin(An)$ for $A = 1, 3, 5$. The markers indicate the values of the functions evaluated for $n \in \mathbb{N}^+$.

Auxiliary model

The equation (S11) is not transparent but it can be dramatically simplified for $\lambda \approx \lambda_{\rm cc}$. Indeed, let $F(\lambda) = \sin(An) - f(\lambda, n)$, and rewrite (S11) in the form $F(\lambda) = 0$. By expanding this equation around $\lambda = \lambda_{\rm cc}$ we obtain $F(\lambda_{\rm cc}, n) + F'(\lambda_{\rm cc}, n)(\lambda - \lambda_{\rm cc}) = 0$ from where the critical wavenumber can be computed as

$$n_{\rm cr} = \arg\max_{\mathbb{N}^+} \left(\frac{\gamma(\lambda_{\rm cc})^2 \sin(n\tilde{A}(\lambda_{\rm cc}))}{n\gamma(\lambda_{\rm cc})^2 \tilde{A}'(\lambda_{\rm cc}) \cos(n\tilde{A}(\lambda_{\rm cc})) - \gamma(\lambda_{\rm cc})\delta(\lambda_{\rm cc}) S'(\lambda_{\rm cc}) \sinh(nB(\lambda_{\rm cc}))} \right) \tag{S13}$$

where

$$S(\lambda) = \frac{\left(1 + \lambda^3\eta(\lambda)\right)}{\left(1 - \lambda^3\eta(\lambda)\right)}, \qquad B(\lambda) = \frac{\pi\gamma(\lambda)}{\lambda^2}\frac{H}{L}.$$

Consider next the limit $H/L \to \infty$. Then we can neglect the cosine carrying term in the denominator of (S13) and approximate the remaining part of the denominator by the the exponential term of the form e^{Bn}, where B turns our to be an irrelevant parameter as far as the limiting behavior at large H/L is concerned, with the right asymptotic behavior already recoverable at $B = 1$.

We can then introduce an auxiliary problem:

$$N(A) \coloneqq \arg\max_{n \in \mathbb{N}^+} \left(e^{-n}\sin(An) \right), \tag{S14}$$

see Fig. S1 showing the optimized function at several values of parameter A. It also illustrates the complexity of the problem (S14) which implies integer valued optimization.

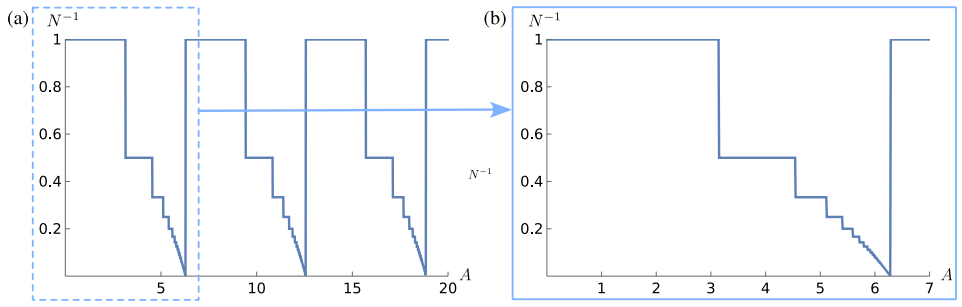

FIG. S2. Plot of the inverse of $N(A)$ over three periods (a) and a zoom over one period (b).

From the boundeness and the periodicity of $\sin(An)$, it follows that the integer valued function $N(A)$ is well defined and non-negative. Since $N(A)$ is periodic with period 2π, it is sufficient to analyze its behavior on the interval $[0, 2\pi]$.

We first show that $N(A) \equiv 1$ if $A \in [0,\, \pi]$. Indeed, by induction in this range of A we have $\frac{\sin(An)}{\sin A} \leq n$. This is clearly true for $n = 1$. Then, if $\sin(An) \leq n \sin(A)$ we obtain $\frac{\sin(A(n+1))}{\sin A} = \frac{\sin(An)\cos A}{\sin A} + \cos(An) \leq n + 1$. Thus, $e^{-n} \sin An \leq e^{-n} n \sin A \leq e^{-1} \sin A$ which proves the result. We next show that $\lim_{A\to 2\pi^-} N(A) = +\infty$. Indeed, for any $M \in \mathbb{N}^+$ we can take $\delta = \pi/M$, and then $\sin(An) < 0$ for all $n \leq M$ and $A \in (2\pi - \delta,\, 2\pi)$. Since the maximum over n of $e^{-n}\sin(An)$ exists and is positive, $N(A) > M$ for $A \in (2\pi - \delta,\, 2\pi)$. This result also proves the periodic blow up of $N(A)$ at $A \to 2m\pi^-$ with $m \in \mathbb{N}^+$, which is in agreement with the behavior of the function $n_{\rm cr}$ obtained numerically, see Fig. S2. Next we show that the integer valued function $N(A)$, apparently exhibiting 'devilish' features around the points $2m\pi^-$ in Fig. S2, indeed takes all positive integer values as the parameter A changes inside the interval of periodicity, $A \in [0,\, 2\pi]$. Suppose that that $N(A) = m$ at some $A = A_m$. If $A_m \in I_m = [2\pi - \pi/m,\, 2\pi]$, then $\sin(A_m l) \leq 0$ whenever $l \leq m$ and $l \in \mathbb{N}^+$. Therefore, $N(A) > m$ in I_m. Our conjecture follows from the observation that $N(A) = m + 1$ for $A_{m+1} = 2\pi - \pi/m$, which can be checked by direct substitution

$$N(A_{m+1}) = \underset{n\in\mathbb{N}^+}{\arg\max} \left(e^{-n} \sin\left(\left(2\pi - \frac{\pi}{m}\right) n\right)\right) = m + \underset{l\in\mathbb{N}^+}{\arg\max} \left(e^{-l} \sin\left(\frac{\pi}{m} l\right)\right) = m + 1,$$

where we used the fact that $\arg\max_{l\in\mathbb{N}^+} \left(e^{-l}\sin\left(l\pi/m\right)\right) = 1$ since $\pi/m \in [0,\, \pi]$.

Weakly nonlinear stability analysis

Near necking. In this case, the critical threshold $\lambda_{\rm cr}$ is a non-degenerate stationary point of the marginal stability curve (λ,n). Accordingly, a small increase of order ε^2 beyond this critical threshold actives a narrow bandwidth of order ε of marginally stable modes. Thus, we can use the order parameter $\varepsilon = \sqrt{(\lambda - \lambda_{\rm cr})/\lambda_{\rm cr}} \ll 1$ to expand the weakly nonlinear terms in the energy functional. The second order equilibrium equations and the incompressibility constraint take the form:

$$K^{(1)}_{jikl} u^{(2)}_{k,lj} + K^{(2)}_{jiklnm} u^{(1)}_{m,n} u^{(1)}_{k,lj} + p^{(2)}_{,i} - p^{(1)}_{j} u^{(1)}_{j,i} = 0 \tag{S15}$$

$$\operatorname{div} \mathbf{u}^{(2)} = u^{(1)}_{1,2} u^{(1)}_{2,1} - u^{(1)}_{2,2} u^{(1)}_{1,1}. \tag{S16}$$

Here $K^{(2)}_{ijklnm} = \sum_{a,\,b,\,c=1}^{2} F_{i\alpha} F_{kb} F_{nc} \frac{\partial^3 W}{\partial F_{ja} \partial F_{lb} \partial F_{mc}}$ are the third-order instantaneous elastic moduli. Similarly, we can obtain the second-order boundary conditions.

The solution of the resulting boundary value problem, implying quadratic coupling with the first order solution, can be written in the form $u^{(2)}_i = U^{(2)}_i(\gamma x_2)|A|^2 + \left(V^{(2)}_i(\gamma x_2) A^2\, e^{2\imath k x_1} + c.c.\right)$, where we introduced the scalar fields $U^{(2)}_i = U^{(2)}_i(\gamma x_2)$ and $V^{(2)}_i = V^{(2)}_i(\gamma x_2)$ which are known explicitly but the corresponding expressions are too cumbersome to be presented here.

A further series development of the solution would introduce resonant terms in the third-order problem due to the cubic interactions of the linear modes. The corresponding solutions can be obtained by requiring that the energy functional is stationary at each relevant order in ε as described it is described in detail for instance in [2].

If we now expand the elastic energy about the homogeneous solution

$$G(\mathbf{u}) = \mathcal{W}(\mathbf{u}) - \mathcal{W}(\mathbf{u}^{(0)}) = \int_\Omega \left[p u_{i,i} + \frac{1}{2} K^{(1)}_{jilk} u_{k,l} u_{i,j} + \frac{1}{6} K^{(2)}_{jilknm} u_{k,l} u_{i,j} u_{m,n} + \frac{1}{24} K^{(3)}_{jilknmqs} u_{k,l} u_{i,j} u_{m,n} u_{s,q} \right] \mathrm{d}V, \tag{S17}$$

where $K^{(3)}_{jilknmqp}$ are the fourth-order instantaneous elastic moduli, and substitute into (S17) the series expansion of the displacement and pressure fields while using (S15) as well as the incompressibility condition at order ε^4 in the form $u^{(4)}_{i,i} = u^{(1)}_{j,k} u^{(3)}_{k,j} + \frac{1}{2} u^{(2)}_{j,k} u^{(2)}_{k,j} - \frac{1}{2}(u^{(2)}_{i,i})^2$, we obtain :

$$\begin{aligned} G(\mathbf{u}) = \varepsilon^4 \int_\Omega \Bigg[& \frac{1}{2} p^{(0)} u^{(2)}_{j,k} u^{(2)}_{k,j} + \frac{1}{2} p_1 u^{(1)}_{j,k} u^{(1)}_{k,j} - \frac{1}{8} p^{(0)} (u^{(1)}_{j,k} u^{(1)}_{k,j})^2 \\ & + p_1 u^{(1)}_{j,k} u^{(2)}_{k,j} + \frac{1}{2} K^{(1)}_{jilk} u^{(2)}_{k,l} u^{(2)}_{i,j} + \frac{1}{2} K^{\star}_{jilk} u^{(1)}_{k,l} u^{(1)}_{i,j} + \\ & \frac{1}{2} K^{(2)}_{jilknm} u^{(1)}_{k,l} u^{(1)}_{i,j} u^{(2)}_{m,n} + \frac{1}{24} K^{(3)}_{jilknmqs} u^{(1)}_{k,l} u^{(1)}_{i,j} u^{(1)}_{m,n} u^{(1)}_{s,q} \Bigg] \mathrm{d}V + O(\varepsilon^4) \end{aligned} \tag{S18}$$

where $p_1 = (dp^{(0)}/d\lambda)|_{\lambda=\lambda_{\rm cr}}$, $K^{\star}_{jilk} = (\partial K^{(1)}_{jilk}/\partial\lambda)|_{\lambda=\lambda_{\rm cr}}$. Observe that the terms of order ε^3 vanish due to periodic nature of the boundary conditions in the horizontal direction. Note also that the next-to-leading term of order ε^4 accounts for the sub-harmonic resonance of the critical mode. In view of the the periodicity of this mode, it is sufficient to perform the integration in (S18) over a critical wavelength. We finally obtain

$$G/\varepsilon^4 = \theta_2 \left|A\right|^2 + \theta_4 \left|A\right|^4 + O(\varepsilon) \tag{S19}$$

where θ_2, θ_4 are known real constants. In particular, θ_2 is a function only of the critical incremental solution, while θ_4 also depends on the subharmonic near-critical mode.

The amplitude equation now follows from the condition that the incremental energy G is stationary (at the lowest nontrivial order ε^4) which means that $dG/dA = 0$ and $\theta_2 A + 2\theta_4 A \left|A\right|^2 = 0$. Combined with its complex conjugate, this equation shows that the bifurcation is of a pitchfork type [3]. Since θ_2 and θ_4 are found having the same sign, the pitchfork is subcritical.

Near wrinkling. In this case, the critical threshold $\lambda_{\rm cr}$ is a degenerate stationary point of the marginal stability curve (λ,n). Accordingly, a small increase of order ε beyond this critical threshold actives an infinite bandwidth of marginally unstable modes. Thus, the weakly nonlinear analysis requires a different scaling comparing to the 'near necking' case. By choosing $\varepsilon = \frac{\lambda-\lambda_{\rm cr}}{\lambda_{\rm cr}} \ll 1$ we can capture the the superposition of all subharmonic modes representing incremental fields, see [4] for a similar analysis and additional references. Thus, the first order terms have now the following structure

$$u_1^{(1)} = \imath \sum_{m=-\infty}^{+\infty} A_m g'(\gamma_{\rm cr} m x_2) e^{\imath\gamma m x_1}, \qquad u_2^{(1)} = \sum_{m=-\infty}^{+\infty} A_m g(\gamma_{\rm cr} m x_2) e^{\imath\gamma m x_1}, \tag{S20}$$

$$p^{(1)} = \sum_{m=-\infty}^{+\infty} A_m m\gamma((K^{(1)}_{1122} + K^{(1)}_{2112} - K^{(1)}_{1111}) g'(\gamma_{\rm cr} m x_2) + K^{(1)}_{2121} g'''(\gamma_{\rm cr} m x_2)) e^{\imath\gamma m x_1}, \tag{S21}$$

where m is an integer and A_m is the amplitude of mode m.

From the linear stability analysis we know that $A_{-m} = \bar{A}_m$, $A_0 = 0$ and $g(-\gamma_{\rm cr} m x_2) = \bar{g}(\gamma_{\rm cr} m x_2)$. By expanding the energy functional (S17), at the next-to-leading order we find

$$G = \frac{\varepsilon^3}{2} \int_\Omega \left[p_1 u^{(1)}_{i,j} u^{(1)}_{j,i} + K^{\star}_{jikl} u^{(1)}_{i,j} u^{(1)}_{l,k} + p^{(1)} u^{(1)}_{i,j} u^{(1)}_{j,1} + \frac{1}{3} K^{(2)}_{jiklqp} u^{(1)}_{i,j} u^{(1)}_{l,k} u^{(1)}_{p,q} \right] {\rm d}V + o(\varepsilon^3). \tag{S22}$$

where we account for the fact that cubic resonances between each of the infinitely many linearly unstable modes become dominant at order ε^3. Using the solution of the incremental (first-order) equilibrium problem which we do not present in full detail here and which specifies the unknown functions in (S20,S21), we obtain

$$\frac{2G}{\varepsilon^3} = \sum_{m=-\infty}^{+\infty} \theta_1(m) |A_m|^2 + \sum_{r=-\infty}^{+\infty} \theta_3(r,m) \bar{A}_m A_r A_{m-r} + o(1), \tag{S23}$$

Here $\theta_1(m)$ and $\theta_3(r,\, m)$ are known real constants which are known functionals of the incremental first-order solutions. We remark that in our case the subharmonic resonance of the critical modes turn out to be appearing only at order ε^4, and can be therefore neglected in the analysis of the amplitude equation. The latter can be obtained from (S23) using the same reasoning as in the 'near necking' case. Specifically, the stationarity of the energy functional (S23) with respect to each amplitude A_m gives

$$\theta_1(m) A_m + \sum_{r=-\infty}^{+\infty} \theta_3(r,m) A_r A_{m-r} = 0, \tag{S24}$$

which is exactly the amplitude equation presented in the main text. To construct the graphs presented in the main paper we solved a truncated system up to a finite order M until a given convergence is reached, adapting the numerical procedure proposed in [5].

Regularized model

In our numerical simulations we use the energy density accounting for both, phase field type regularization and weak compressibility:

$$\begin{aligned} w_{\rm pf}(\alpha,\,\mathsf{F}) &= a(\alpha)w_J(\mathsf{F}) + \phi(\alpha) + \phi(1)\ell^2\|\nabla\alpha\|^2, \\ w_J(\mathsf{F}) &= \frac{\mu}{I}\,(I-2-2\log J) + \frac{\Lambda}{2}(\log J)^2. \end{aligned} \tag{S25}$$

We remark that, as the auxiliary field α increases, the shear modulus of the material diminishes but its compressibility is not affected. In all the simulations, the parameter Λ was set equal to 100μ.

The fully non linear problem was approximated using the finite element method. We discretize the displacement field by using continuous piecewise quadratic functions to avoid locking phenomena. On the other hand, the auxiliary field α is approximated by piecewise linear functions.

We decompose the displacement field into two components $\mathbf{u}(\mathbf{x}) = \mathbf{u}^{(0)}(\mathbf{x}) + \delta\mathbf{u}(\mathbf{x})$, where $\mathbf{u}^{(0)}$ is the homogeneous solution. This choice is motivated by the fact that we can impose homogeneous boundary conditions on the displacement field $\delta\mathbf{u}$, simplifying the implementation of the continuation method. The deformation gradient becomes $\mathsf{F} = \mathsf{I} + \nabla\mathbf{u} = \mathsf{I} + \nabla\mathbf{u}^{(0)} + \nabla\delta\mathbf{u}$. In order to select the bifurcated branch in the post-bifurcation regime, a small imperfection is imposed at the boundary of the domain with the amplitude of the order of $10^{-5}\,L$. The wavenumber of the imperfection is chosen to match the nontrivial eigenfunction of linear stability analysis.

Then, we use the arclength continuation method [6] to construct the bifurcation diagram and to study the post-bifurcational behavior.

The method was implemented in Python using the software collection for the numerical solution of partial differential equations FEniCS [7], the library BiFEniCS [8][9] for the arclength continuation method, while PETSc was used as linear algebra backend [10]. The nonlinear problem was numerically solved through a SNES solver, where a secant predictor was used to identify the initial guess. At each step of the non-linear algorithm, the linear system was directly solved using MUMPS. The computational domain was discretized by subdividing each side of the rectangle into intervals of length $L/250$ and constructing a structured triangular mesh.

The geometrically linear case

Suppose that the deformation of our isotropic material is (geometrically) small but the material response is still (physically) nonlinear. Let E_1 and E_2 be the eigenvalues of the infinitesimal strain tensor $\mathsf{E} = \operatorname{sym}\nabla\mathbf{u} = (1/2)(\nabla\mathbf{u} + \nabla\mathbf{u}^T)$. Then the strain energy density is $w(E_1,\,E_2)$. In this geometrical nonlinear approximation the incompressibility constraint reduces to $\operatorname{tr}\mathsf{E} = \nabla\cdot\mathbf{u} = 0$ and therefore, without loss of generality, we canassume that $0 < E = E_1 = -E_2$, and introduce the reduced energy density $\hat{w}(E) = w(E,\,-E)$. We observe that $\hat{w}' = w_{,1} - W_{,2}$, and $\hat{w}'' = w_{,11} + w_{,22} - 2w_{,12}$, where $w_{,j} = \partial w/\partial E_j$. The Cauchy stress tensor is then $\mathsf{S} = \partial w/\partial\mathsf{E} + p\mathsf{I}$.

In the case of uniaxial traction, the homogeneous solution of the elastic equilibrium problem is $\mathbf{u}^{(0)} = EX_1\mathbf{e}_1 - EX_2\mathbf{e}_2$ and $p^{(0)} = -w_{,2}$. To study linear stability of such a solution, we again we expand the unknown functions in terms of the small parameter ε. Thus, we can write $\mathsf{S} = \sum_j \varepsilon^j\mathsf{S}^{(j)}$, where $\mathsf{S}^{(1)} = \mathbf{C}^{(1)} : \mathsf{E}^{(1)} + p^{(1)}\mathsf{I}$, while $\mathsf{E}^{(j)} = \operatorname{sym}\nabla\mathbf{u}^{(j)}$, and $\mathbf{C}^{(1)} = \left.\frac{\partial^2 W}{\partial\mathsf{E}\partial\mathsf{E}}\right|_{\mathsf{E}^{(0)}}$. Using the results of [11] we obtain that $C^{(1)}_{iijj} = w_{,ij}$, and $C^{(1)}_{ijij} = \frac{1}{2}\frac{w_{,i}-w_{,j}}{e_i-e_j}$ for $i \neq j$, while all the other components of the tensor $\mathbf{C}^{(1)}$ are equal to zero. The linearized form of the balance of the linear momentum and of the incompressibility constraint reads

$$\nabla\cdot\mathsf{S}^{(1)} = 0 \qquad \operatorname{tr}\mathsf{E}^{(1)} = 0.$$

Using again the stream function χ, we can write $\mathbf{u}^{(1)} = \partial\chi/\partial x_2\mathbf{e}_1 - \partial\chi/\partial x_1\mathbf{e}_2$ where now $\chi = \imath Ag(\gamma x_2)e^{\imath\gamma x_1}/\gamma$. The function $g(\gamma x_2)$ is a solution of the ODE

$$ag''''(\gamma x_2) - 2bg''(\gamma x_2) + cg(\gamma x_2) = 0,$$

where $a = c = \frac{\hat{w}'}{2E}$, and $b = w'' - \frac{\hat{w}'}{2E}$. The corresponding characteristic equation takes the form

$$\left(\alpha^2+1\right)\left(\beta^2+1\right)\left(\alpha\beta\left(\alpha^2+\beta^2+2\right)\left(\cosh(\alpha\gamma H)\cosh(\beta\gamma H)-1\right) - \left(\alpha^2\left(2\beta^2+1\right)+\beta^2\right)\sinh(\alpha\gamma H)\sinh(\beta\gamma H)\right) = 0$$

where α and β are defined as in (S4) while the solution $g(\gamma x_2)$ has the same form as (S3).

We observe that the load maximum condition corresponds to a strain $E_{\rm lm}$ such that $w''(E_{\rm lm}) = 0$,representing a necessary condition for a bifurcation to occur [12]. Similarly a sufficient condition for the instability of any wavenumber is provided by the condition of loss of strong ellipticity, which is reached at $b = -\sqrt{ac}$ [1], i.e. when $E = E_{\rm sm}$ defined again by the same condition $w''(E_{\rm se}) = 0$. Therefore, a bifurcation occurs if and only if $E = E_{\rm lm} = E_{\rm se}$ for any value of γ, and all the wavenumbers become unstable simultaneously.

* lev.truskinovsky@espci.fr

[1] R. W. Ogden, *Non-Linear Elastic Deformations* (Dover, 1984).
[2] B. Budiansky, Adv. Appl. Mech. **14**, 1 (1974).
[3] F. Charru, *Hydrodynamic instabilities*, Vol. 37 (Cambridge University Press, 2011).
[4] P. Ciarletta and Y. Fu, Int. J. Non-Linear Mech. **75**, 38 (2015).
[5] Y. B. Fu and P. Ciarletta, Proc. R. Soc. A **471**, 20140979 (2015).
[6] R. Seydel, *Practical bifurcation and stability analysis*, Vol. 5 (Springer Science & Business Media, 2009).
[7] M. Alnæs, J. Blechta, J. Hake, A. Johansson, B. Kehlet, A. Logg, C. Richardson, J. Ring, M. E. Rognes, and G. N. Wells, Archive of Numerical Software **3**, 9 (2015).
[8] D. Riccobelli, G. Noselli, and A. DeSimone, Proc. R. Soc. A **477**, 20200817 (2021).
[9] `https://github.com/riccobelli/bifenics`.
[10] S. Balay, S. Abhyankar, M. Adams, P. Brune, K. Buschelman, L. Dalcin, W. Gropp, B. Smith, D. Karpeyev, D. Kaushik, *et al.*, *Petsc users manual revision 3.7*, Tech. Rep. (Argonne National Lab.(ANL), Argonne, IL (United States), 2016).
[11] P. Chadwick and R. W. Ogden, Arch. Rational Mech. Anal. **44**, 54 (1971).
[12] R. Hill and J. Hutchinson, J. Mech. Phys. Solids **23**, 239 (1975).